Generalized Autoencoder: A Neural Network Framework for Dimensionality Reduction

Wei Wang[1], Yan Huang[1], Yizhou Wang[2], Liang Wang[1]
[1]Center for Research on Intelligent Perception and Computing, CRIPAC
Nat'l Lab of Pattern Recognition, Institute of Automation Chinese Academy of Sciences
[2]Nat'l Eng. Lab for Video Technology, Key Lab. of Machine Perception (MoE),
Sch'l of EECS, Peking University, Beijing, China
{wangwei, yhuang, wangliang}@nlpr.ia.ac.cn, yizhou.wang@pku.edu.cn

Abstract

The autoencoder algorithm and its deep version as traditional dimensionality reduction methods have achieved great success via the powerful representability of neural networks. However, they just use each instance to reconstruct itself and ignore to explicitly model the data relation so as to discover the underlying effective manifold structure. In this paper, we propose a dimensionality reduction method by manifold learning, which iteratively explores data relation and use the relation to pursue the manifold structure. The method is realized by a so called "generalized autoencoder" (GAE), which extends the traditional autoencoder in two aspects: (1) each instance x_i is used to reconstruct a set of instances $\{x_j\}$ rather than itself. (2) The reconstruction error of each instance ($||x_j - x'_i||^2$) is weighted by a relational function of x_i and x_j defined on the learned manifold. Hence, the GAE captures the structure of the data space through minimizing the weighted distances between reconstructed instances and the original ones. The generalized autoencoder provides a general neural network framework for dimensionality reduction. In addition, we propose a multilayer architecture of the generalized autoencoder called deep generalized autoencoder to handle highly complex datasets. Finally, to evaluate the proposed methods, we perform extensive experiments on three datasets. The experiments demonstrate that the proposed methods achieve promising performance.

1. Introduction

Real-world data, such as images of faces and digits, usually have a high dimension which leads to the well-known *curse of dimensionality* in statistical pattern recognition. However, high dimensional data usually lies in a lower dimensional manifold, so-called "intrinsic dimensionality space". Various methods of dimensionality reduction have been proposed to discover the underlying manifold structure, which plays an important role in many tasks, such as pattern classification [9] and information visualization [16].

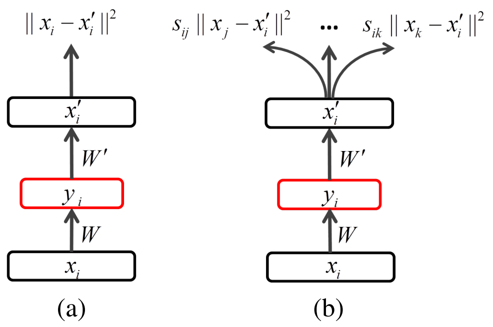

Figure 1. Traditional autoencoder and the proposed generalized autoencoder. (a) In the traditional autoencoder, x_i is only used to reconstruct itself and the reconstruction error $||x_i - x'_i||^2$ just measures the distance between x_i and x'_i. (b) In the generalized autoencoder, x_i involves in the reconstruction of a set of instances $\{x_j, x_k, ...\}$. Each reconstruction error $s_{ij}||x_j - x'_i||^2$ measures a weighted distance between x_j and x'_i.

Principal Component Analysis (PCA) is one of the most popular linear dimensionality reduction techniques [10][17]. It projects the original data onto its principal directions with the maximal variance, and does not consider any data relation.

Linear Discriminant Analysis (LDA) is a supervised method to find a linear subspace, which is optimal for discriminating data from different classes [2]. Marginal Fisher Analysis (MFA) extends LDA by characterizing the intraclass compactness and interclass separability [19]. These two methods use class label information as a weak data relation to seek a low-dimensional separating subspace.

However, the low-dimensional manifold structure of real data is usually very complicated. Generally, just using a simple parametric model, such as PCA, it is not easy to capture such structures. Exploiting data relations has been proved to be a promising means to discover the underlying structure. For example, ISOMAP [15] learns a low-dimensional manifold by retaining the geodesic distance between pairwise data in the original space. In Locally Linear Embedding (LLE) [12], each data point is a linear combination of its neighbors. The linear relation is preserved in the projected low-dimensional space. Laplacian Eigenmaps (LE) [1] purses a low-dimensional manifold by minimizing the pairwise distance in the projected space weighted by the corresponding distance in the original space. They have a common weakness of suffering from the out-of-sample problem. Neighborhood Preserving Embedding (NPE) [3] and Locality Preserving Projection (LPP) [4] are linear approximations to LLE and LE to handle the out-of-sample problem, respectively.

Although these methods exploit local data relation to learn manifold, the relation is fixed and defined on the original high-dimensional space. Such relation may not be valid on the manifold, e.g. the geodesic nearest neighbor on a manifold may not be the Euclidian nearest neighbor in the original space.

The autoencoder algorithm [13] belongs to a special family of dimensionality reduction methods implemented using artificial neural networks. It aims to learn a compressed representation for an input through minimizing its reconstruction error. Fig.1(a) shows the architecture of an autoencoder. Recently, the autoencoder algorithm and its extensions [8][18][11] demonstrate a promising ability to learn *meaningful features* from data, which could induce the "intrinsic data structure". However, these methods just consider self-reconstruction and ignore to explicitly model the data relation.

In this paper, we propose a method of dimension reduction by manifold learning, which extends the traditional autoencoder to iteratively explore data relation and use the relation to pursue the manifold structure. The proposed method is realized by a so called "generalized autoencoder" (GAE). As shown in Fig.1, it differs from the traditional autoencoder in two aspects, (i) the GAE learns a compressed representation y_i for an instance x_i, and builds the relation between x_i and other data $\{x_j, x_k ...\}$ by using y_i to reconstruct each element in the set, not just x_i itself. (ii) The GAE imposes a relational weight s_{ij} on the reconstruction error $||x_j - x_i'||^2$. Hence, the GAE captures the structure of the data space through minimizing the weighted reconstruction error. When replacing the sigmoid function in the GAE with a linear transformation, we show that the linear GAE and the linear graph embedding [19] have similar objective functions. This indicates that the GAE can also be a general framework for dimensionality reduction by defining different reconstruction sets and weights. Inspired by existing dimensionality reduction ideas, we derive six implementations of GAE including both supervised and unsupervised models. Furthermore, we propose a deep GAE (dGAE), which extends GAE to multiple layers.

The rest of the paper is organized as follows. In Section 2, we first introduce the formulation of the generalized autoencoder and its connection to graph embedding, then propose the generalized autoencoder as a general framework of dimensionality reduction and derive its six implementations. In Section 2.3, we illustrate deep generalized autoencoder as a multilayer network of GAE. The experimental results on three datasets are presented in Section 3. Finally, we discuss the proposed method and conclude the paper in Section 4.

2. Dimensionality Reduction by Manifold Learning

2.1. The method

Algorithm 1 shows the proposed method. (1) We initialize the data relation by computing the data pairwise similarity/distance in the original high dimension space, then determine a "relation/reconstruction" set Ω_i for each data point x_i. For example, the set can be composed of k-nearest neighbors. (2) Local manifold structure around each data is learned from its reconstruction set using the proposed "generalized autoencoder" (GAE) introduced below. (3) On the learned manifold, data relation is updated according to the pairwise similarity/distance defined on the hidden representation derived from the GAE. Step (2) and (3) are iterated until convergence or the maximum iteration number being reached.

2.2. Generalized Autoencoder

The generalized autoencoder consists of two parts, an encoder and a decoder. As shown in Fig. 1 (b), the encoder maps an input $x_i \in \mathcal{R}^{d_x}$ to a reduced hidden representation $y_i \in \mathcal{R}^{d_y}$ by a function $g()$,

$$y_i = g(Wx_i) \tag{1}$$

where $g()$ is either the identity function for a linear projection or a sigmoid function $\frac{1}{1+e^{-Wx}}$ for a nonlinear mapping. The parameter W is a $d_y \times d_x$ weight matrix. In this paper, we ignore the bias terms of the neural network for simple notation.

The decoder reconstructs $x_i' \in \mathcal{R}^{d_x}$ from the hidden representation y_i

$$x_i' = f(W'y_i) \tag{2}$$

The parameter W' is another $d_x \times d_y$ weight matrix, which can be W^T. Similar to $g()$, $f()$ is either the identity function

Algorithm 1 Iterative learning procedure for Generalized Autoencoder

```
Input: training set $\{x_i\}_1^n$
Parameters: $\Theta = (W, W')$
Notation: $\Omega_i$: reconstruction set for $x_i$
          $S_i$: the set of reconstruction weight for $x_i$
          $\{y_i\}_1^n$: hidden representation
1. Compute the reconstruction weights $S_i$ from $\{x_i\}_1^n$ and
   determine the reconstruction set $\Omega_i$, e.g. by $k$-nearest
   neighbor
2. Minimize $E$ in Eqn.4 using the stochastic gradient
   descent and update $\Theta$ for $t$ steps
3. Compute the hidden representation $\{y_i\}_1^n$, and update
   $S_i$ and $\Omega_i$ from $\{y_i\}_1^n$ .
4. Repeat step 2 and 3 until convergence.
```

for a linear reconstruction or a sigmoid function for a binary reconstruction.

To model the relation between data, the decoder reconstructs a set of instances indexed by $\Omega_i = \{j, k...\}$ with specific weights $S_i = \{s_{ij}, s_{ik}...\}$ for x_i. The weighted reconstruction error is

$$e_i(W, W') = \sum_{j \in \Omega_i} s_{ij} L(x_j, x'_i) \tag{3}$$

where L is the reconstruction error. Generally, the squared error $L(x_j, x'_i) = ||x_j - x'_i||^2$ is used for linear reconstruction and the cross-entroy loss $L(x_j, x'_i) = -\sum_{q=1}^{d_x} x_j^{(q)} log(x_i'^{(q)}) + (1 - x_j^{(q)}) log(1 - x_i'^{(q)})$ for binary reconstruction [5].

The total reconstruction error E of n samples is

$$E(W, W') = \sum_{i=1}^{n} e_i(W, W') = \sum_{i=1}^{n} \sum_{j \in \Omega_i} s_{ij} L(x_j, x'_i) \tag{4}$$

The generalized autoencoder learns the parameters (W, W') via minimizing E.

2.2.1 Connection to Graph Embedding

Graph embedding [19] is known to be a general framework for dimensionality reduction, of which each data is represented as a graph node in a low-dimensional vector, the edges preserve similarities between the data pairs. The similarities characterize certain statistical or structural properties of data distribution. The formulation of graph embedding is

$$y^* = \arg \min_{y^T B y = c} \sum_{i,j} s_{ij} ||y_i - y_j||^2, \tag{5}$$

where y is the low-dimensional representation. s_{ij} is the similarity between the vertex i and j, usually, $s_{ij} = s_{ji}$. c is a constant and B is a constraint matrix to avoid a trivial solution [1].

The linear graph embedding (LGE) assumes that the low-dimensional representation can be obtained by a linear projection $y = X^T w$, where w is the projection vector and $X = [x_1, x_2, ..., x_n]$. The objective function of LGE is

$$w^* = arg \min_{\substack{w^T X B X^T w = c \\ \text{or } w^T w = c}} \sum_{i,j} s_{ij} ||w^T x_i - w^T x_j||^2 \tag{6}$$

Similarly, the hidden representation of the generalized autoencoder induces a low-dimensional manifold of data when $d_y < d_x$, on which the relation/similarity/distance between data pairs is defined through one reconstructing the others. From Eqn.2,1,4, the total reconstruction error E is

$$(W, W')^* = \arg\min \sum_{i,j} s_{ij} ||x_j - f(W' g(W x_i))||^2 \tag{7}$$

In the linear reconstruction case, if $W' = W^T$ (like [11]) and assuming only one hidden node in the network, i.e. $d_y = 1$, W degenerates to a column vector w, the objective function Eqn. 7 becomes

$$w^* = \arg\min \sum_{i,j} s_{ij} ||x_j - w w^T x_i||^2 \tag{8}$$

Let $w^T w = c$ and $y_i = w^T x_i$, Eqn. 8 becomes

$$w^* = \arg \min_{w^T w = c} \sum_{i,j} s_{ij} (||w^T x_i - w^T x_j||^2 + (\frac{c}{2} - 1) y_i^2) \tag{9}$$

Compared with the linear graph embedding (LGE) Eqn. 6, we can see that the generalized autoencoder (GAE) has an additional term which controls different tuning behaviors over the hidden representation y by varying c. If $c = 2$, the GAE has the similar objective function to LGE. If $c > 2$, this term prevents y being too large, even if the norm of w could be large. If $c < 2$, this term encourages y to be large enough when w is small.

The linear version of the above models just illustrates the connection between the generalized autoencoder and the graph embedding. In real applications, $g()$ in the generalized autoencoder is usually preferred to be nonlinear due to its powerful representability.

2.2.2 Implementation of the GAE Variants

As can be seen from the above analysis, the generalized autoencoder can also be a general framework for dimensionality reduction through defining different reconstruction sets and weights. In the following, we derive six implementations of the GAE inspired by previous dimensionality reduction ideas, namely PCA [10], LDA [2], ISOMAP [15], LLE [12], LE [1] and MFA [19].

[1]Original constraint $i \neq j$ is not used here, because $i = j$ does not violate the objective function

Table 1. Six implementations of the generalized autoencoders inspired by PCA [10], LDA [2], ISOMAP [15], LLE [12], LE [1] and MFA [19]

Method	Reconstruction Set	Reconstruction Weight
GAE-PCA	$j = i$	$s_{ij} = 1$
GAE-LDA	$j \in \Omega_{c_i}$	$s_{ij} = \frac{1}{n_{c_i}}$
GAE-ISOMAP	$j : x_j \in X$	$s_{ij} \in S = -H\Lambda H/2$
GAE-LLE	$j \in N_k(i)$,	$s_{ij} = (M + M^T - M^T M)_{ij}$ if $i \neq j$;
	$j \in (N_k(m) \cup m), j \neq i$ if $\forall m, i \in N_k(m)$	0 otherwise
GAE-LE	$j \in N_k(i)$	$s_{ij} = \exp\{-\|\|x_i - x_j\|\|^2/t\}$
GAE-MFA	$j \in \Omega_{k_1}(c_i)$,	$s_{ij} = 1$
	$j \in \Omega_{k_2}(\bar{c_i})$	$s_{ij} = -1$

GAE-PCA: an input x_i is used to reconstruct itself with unit weight, *i.e.* $\Omega_i = \{i\}$, $s_{ii} = 1$. Given the constraint $w^T w = 1$, Eqn. 8 can be rewritten as

$$w^* = \arg \max_{w^T w = 1} \sum_i w^T x_i x_i^T w \qquad (10)$$

which is the formulation of traditional PCA with zero mean [2].

The neural network implementation of GAE-PCA is exactly the traditional autoencoder [5], which is a special case of the proposed GAE.

GAE-LDA An input x_i is used to reconstruct all the data from the same class as x_i, *i.e.* $j \in \Omega_{c_i}$ where Ω_{c_i} is the index set of Class c_i, which x_i belongs to. The weight s_{ij} is inversely proportional to the sample size n_{c_i} of class c_i, $s_{ij} = \frac{1}{n_{c_i}}$. The one-dimensional linear GAE-LDA follows Eqn. 9. It should be noted that the GAE-LDA does not need to satisfy the following two constraints as the traditional LDA: (1) data in each class follow Gaussian distribution. (2) The projection dimension is lower than the number of classes.

GAE-ISOMAP An input x_i is used to reconstruct all the data X. Let D_G be the geodesic distances of all the data pairs [15]. The weight matrix $S = -H\Lambda H/2$, where $H = I - \frac{1}{n}ee^T$, e is the n-dimensional **1**-vector, $\Lambda_{ij} = D_G^2(i,j)$ [19]. The one-dimensional linear GAE-ISOMAP follows Eqn. 9.

GAE-LLE An input x_i is used to reconstruct its k-nearest neighbors and some other inputs' k-nearest neighbors which x_i belongs to, *i.e.* $j \in \{N_k(i), N_k(m), m\}$ and $j \neq i$ if $\forall m, i \in N_k(m)$, where $N_k(i)$ is the index set of the k-nearest neighbors of x_i. Let M be the local reconstruction coefficient matrix, and $\sum_{j \in N_k(i)} M_{ij} = 1$, $M_{ij} = 0$ if $j \notin N_k(i)$ [12]. The weight matrix $S_{ij} = (M + M^T - M^T M)_{ij}$ if $i \neq j$; 0, otherwise [19]. The one-dimensional linear GAE-LLE follows Eqn. 9.

GAE-LE An input x_i is used to reconstruct its k nearest neighbors, *i.e.* $j \in N_k(i)$. The reconstruction weight is $s_{ij} = \exp\{-||x_i - x_j||^2/t\}$, where t is a tuning parameter [1]. Given that the objective function of LE is similar to Eqn. 5, the one-dimensional linear GAE-LE follows Eqn. 9.

GAE-MFA An input x_i is used to reconstruct its k_1-nearest neighbors of the same class, and its k_2-nearest neighbors of other classes, *i.e.* if $j \in \Omega_{c_i}^{k_1}$, $s_{ij} = 1$ and if $j \in \Omega_{\bar{c_i}}^{k_2}$, $s_{ij} = -1$, where $\Omega_{c_i}^{k_1}$ is the index set of x_i's k_1-nearest neighbors in Class c_i and $\Omega_{k_2}(\bar{c_i})$ is the index set of x_i's k_2-nearest neighbors in all the other classes. Similar to MFA, the positive reconstruction characterizes the "intraclass compactness" while the negative reconstruction characterizes the "interclass separability".

We give a summary of the reconstruction sets and weights of the six methods in Table 1. As can be seen from this table, we can easily devise new algorithms in this framework by combining the ideas of these methods. For example, when introducing class labels to GAE-LE (or GAE-LLE) and choosing the k-nearest neighbors of the same class as x_i, we can obtain a supervised GAE-LE (or supervised GAE-LLE).

2.3. Deep Generalized Autoencoder

To handle more complex dataset, we extend the generalized autoencoder to a multilayer network called deep generalized autoencoder (dGAE). It contains a multilayer encoder network to transform the high-dimensional input data to a low-dimensional hidden representation and a multilayer decoder network to reconstruct the data. The structures of the two networks are symmetric with respect to the low-dimensional hidden representation layer. For example, Fig. 2(a) shows a five-layer dGAE on a face dataset used in Section 3.3. It has a three-layer encoder network and a three-layer decoder network labeled with a box. They are symmetric with respect to the second hidden layer of 100 real-valued nodes.

In order to obtain good initial weights of the network, we adopt the layer-wise pretraining procedure introduced in [5]. When pretraining the first hidden layer of 200 binary features, the real-valued face data in the input layer is modeled by a Gaussian distribution. The first hidden layer and the input layer are modeled as a Gaussian restrict-

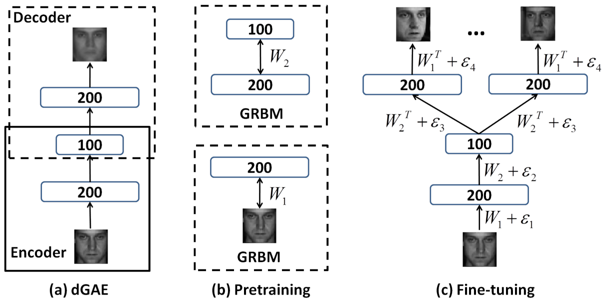

Figure 2. Training a deep generalized autoencoder (dGAE) on the face dataset used in Section 3.3. (a) The dGAE consists of a three-layer encoder network and a three-layer decoder network. A reconstructed face is in the output layer. (b) Pretraining the dGAE through learning a stack of Gaussian restricted Boltzmann machines (GRBM). (c) Fine-tuning a deep GAE-LDA.

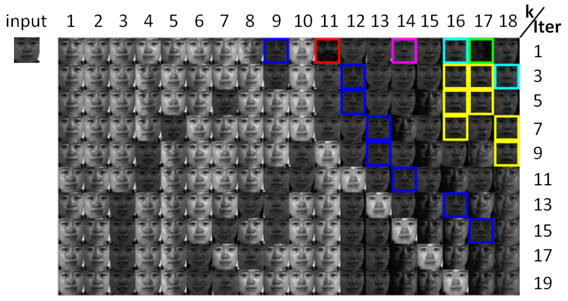

Figure 3. The changes of nearest neighbors during the iterative learning. Each row shows the 18 nearest neighbors of an input data during in one iteration of learning. The faces in the colored boxes belong to other persons. The color indicates the identity of the persons. We can see that along the iterative learning, the nearest neighbors of a data converges to its own class.

ed Boltzmann machine (GRBM) [5]. When pretraining the second hidden layer of 100 real-valued features, the first hidden layer is now considered as the input to the second hidden layer. The first and second hidden layers are combined to form another GRBM as shown in Fig. 2(b). These two GRBMs can be trained efficiently using Contrastive Divergence method [5].

After pretraining, we obtain the weights $\{W_i\}_{i=1,2}$ for both the encoder and the decoder. We further fine-tune them by backpropagating the derivatives of the total reconstruction error in Eqn.4. Fig.2 (c) illustrates the fine-tuning procedure of a deep GAE-LDA (dGAE-LDA) through reconstructing the other faces in the same class.

3. Experimental Results

In this section, we discuss two applications of the GAE, one for face recognition and the other for digit classification. First, we show the effectiveness of manifold learning by the GAE and its extensions.

3.1. Data Sets

Experiments are conducted on three datasets. (1) The face dataset F1 contains 1,965 grayscale face images from the frames of a small video. It is also used in [12]. The size of each image is 20 $\times$ 28 pixels. (2) The CMU PIE face database [14] contains 68 subjects in 41,368 face images. The size of each image is 32 $\times$ 32 pixels. These face images are captured under varying poses, illumination and expression. (3) The MNIST dataset contains 60,000 grayscale images of handwritten digits. The size of each digit image is 28 $\times$ 28 pixels. Considering that computing the reconstruction weights of some of the six GAE implementations, e.g. the geodesic distance of the GAE-ISOMAP, is time consuming when the dataset is large, we randomly select 10,000 images to use in our experiments. For each digit, 500 images are for training and the other 500 are used for testing.

3.2. Manifold Learning

Generally, high-dimensional real data is considered to lie in a low-dimensional space, such as face images and handwritten digit images. Similar to the previous methods [15][1][12], the GAE provides an effective means to discover the nonlinear manifold structure.

Firstly, we explore the ability of the GAE in local manifold structure discovery by checking the changes of the k-nearest neighbors of a data during the iterative learning process. Fig.3 shows the changes of a face's 18 nearest neighbors during the first 20 iterations of our unsupervised dGAE-LE learning on the CMU PIE dataset. Each row shows the 18 nearest neighbors of the input during in one iteration of learning. The faces in the colored boxes belong to other persons. The color indicates the identity of the persons. From the result, it can be seen that along the iteration, the nearest neighbors of the face converges to its own class, and the same person's faces under similar illumination are moving forward. We also compute the average "impurity" change of the 18 nearest neighbors across the dataset during the learning. The *impurity* is defined as the ratio of the number of data from other classes to 18. Fig. 4 shows the decreasing impurity of the first 20 iterations. It indicates that our GAE is able to find more and more reasonably similar neighbors along the learning. Consequently, this may result in a more meaningful local manifold structure.

In addition, we compare the manifold learning results of different models, *i.e.*, LPP [4], dGAE-PCA and dGAE-LE [2], on the F1 dataset. For visualization, we map the face images into a two-dimensional manifold space learned from

[2]Due to limited space, we only show the learned manifolds from dGAE-PCA and dGAE-LE. dGAE-PCA is actually the deep autoencoder [5]. We choose the unsupervised form of dGAE-LE to make a compar-

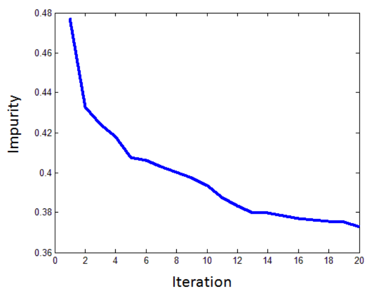

Figure 4. Impurity change during the iterative learning. Impurity is defined as the ratio between the number of data from other classes to the number of the nearest neighbors.

these models. Both of our methods consist of an encoder with layers of size (20×28)-200-2 and a symmetric decoder. The 2D manifolds are shown in Fig. 5. The representative faces are shown next to the data points. As can be seen, the distributions of the data points of our two methods appear radial patterns. Along the radial axes and angular dimension, the facial expression and the pose change smoothly.

We visualize the 2D data manifolds of 0∼9 digit images of the MNIST dataset learned from two unsupervised methods, (*i.e.* the LPP [4], dGAE-LE) and four supervised methods (*i.e.* MFA [19], LDA [2], dGAE-MFA, dGAE-LDA). Fig. 6 shows the results. The data points of the 10 digits are shown with different colors and symbols. Our three methods consist of an encoder with layers of size (28×28)-1000-500-250-2 and a symmetric decoder. As can be seen, the data points of different digits overlap seriously derived from LPP, MFA and LDA. Whereas, data points form more distinctive clusters using the three proposed methods. Moreover, by employing class labels, the clusters from dGAE-MFA, dGAE-LDA are more distinguishable than dGAE-LE.

3.3. Application to Face Recognition

In this section, we evaluate the performance of our six GAEs on the CMU PIE dataset, and compare the results to other four methods and their kernel versions.

Similar to the experiment setting in [4], 170 face images of each individual are used in the experiments, 85 for training and the other 85 for testing. All the images are first projected to a PCA subspace for noise reduction. We retain 98% of the energy in the denoising step and use a 157-dimensional feature for each image. In the experiments, we adopt a 157-200-100 encoder network for the deep generalized autoencoders. After learning the parameters of the deep GAEs, the low-dimensional representations are computed for all the face images. Then, we apply the nearest-neighbor classifier on the learned low-dimensional space to classify the testing data and compute the error rates.

ison with dGAE-PCA. In data visualization, we only show the results of three representative methods, *i.e.*, dGAE-LE as an unsupervised method, dGAE-MFA and dGAE-LDA as two supervised methods.

Table 2. Performance comparison on the CMU PIE dataset. ER is short for "error rate". The reduced dimensions are in parentheses. Our models use 100 dimensions. g and pp are short for "Gaussian" and "polyplus" kernels.

Method	ER	Our Model	ER
PCA	20.6% (150)	dGAE-PCA	3.5%
Kernel PCA	8.1% (g)		
LDA	5.7% (67)	dGAE-LDA	1.2%
Kernel LDA	1.6% (pp)		
ISOMAP	–	dGAE-ISOMAP	2.5%
LLE	–	dGAE-LLE	3.6%
LPP	4.6%(110)	dGAE-LE	1.1%
Kernel LPP	1.7% (pp)		
MFA	2.6% (85)	dGAE-MFA	1.1%
Kernel MFA	2.1% (pp)		

Table 2 shows the recognition results of 14 models on this dataset, namely (kernel) PCA [10], (kernel) LDA [2], (kernel) LPP [4], (kernel) MFA [19] and our six dGAEs. Due to the out-of-sample problem, we cannot give the results of ISOMAP, LLE and LE. However, considering the LPP as a popular linear approximation to the LE, we present the result of the supervised LPP as [4]. Correspondingly, we use the supervised version of dGAE-LE for comparison. For the kernel methods, we present the best performance from Gaussian kernel, polynomial kernel and polyplus kernel[3]. For the other four non-kernel methods, we select the manifold dimensions with the best performance, which is shown in parentheses in Table 2. We select 100 as the manifold dimension for all our dGAEs.

As can be seen, our methods generally perform much better than their counterparts. Three supervised methods dGAE-LDA, dGAE-LE and dGAE-MFA with the error rate 1.2%, 1.1% and 1.1% achieve the best performance. Except for the dGAE-LLE, all the other four dGAEs have a lower error rate than dGAE-PCA (which is a deep autoencoder [5]). This justifies the importance of considering the data relation on the manifold during the iterative learning, which is the motivation of this work. Moreover, the low error rate of dGAE-LDA may indicate that the requirement by the LDA - the data of each class follow a Gaussian distribution - is not longer a necessity.

3.4. Application to Digit Classification

To further evaluate the performance of the proposed GAEs, we classify digits from the MNIST dataset.

[3]The form of polypuls kernel is $K(x, y) = (x'y+1)^d$, d is the reduced dimension.

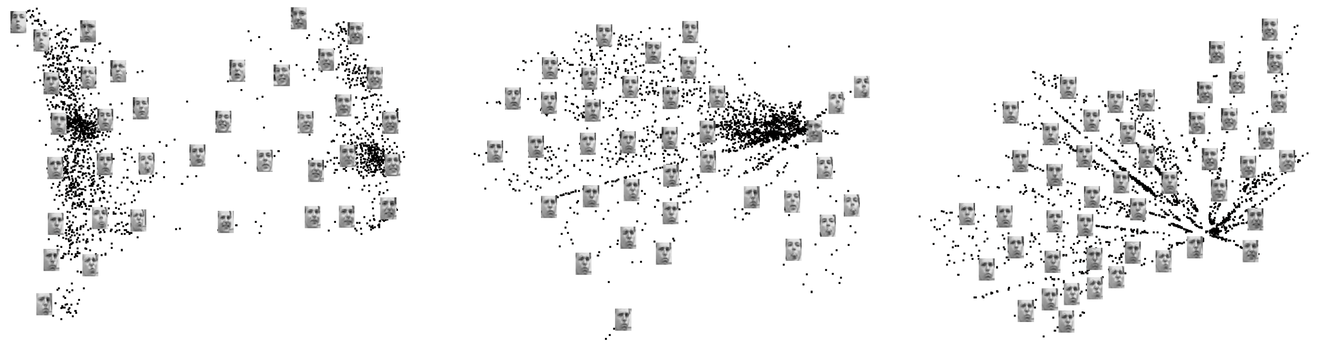

(a) LPP [4] (b) dGAE-PCA (deep autoencoder [5]) (c) dGAE-LE

Figure 5. 2D visualization of the face image manifold on the F1 dataset.

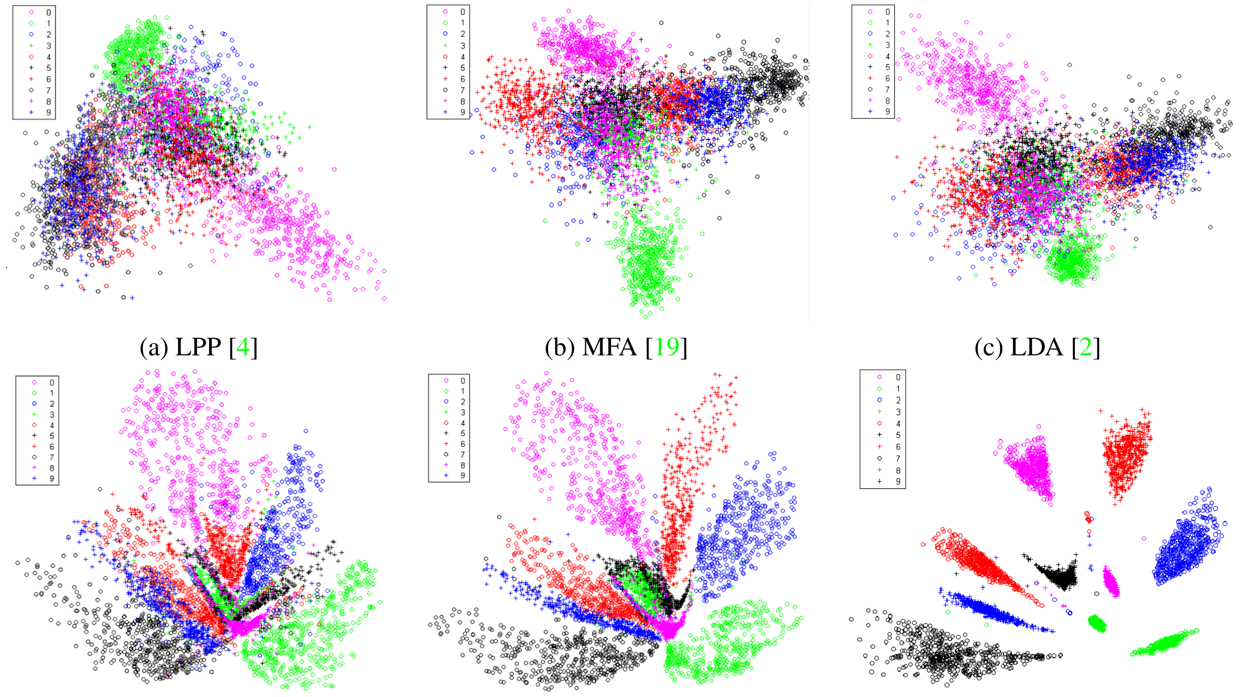

(a) LPP [4] (b) MFA [19] (c) LDA [2]

(d) dGAE-LE (e) dGAE-MFA (f) dGAE-LDA

Figure 6. 2D visualization of the learned digit image manifold.

We use the 784-dimensional raw data as the input. In our deep GAEs, the encoder layers are of the size 784-500-200-30. We adopt the same testing procedure as the face recognition experiments, and the manifold dimension is set to 30 for all the dGAEs.

Table 3 shows the classification results of the 14 methods. The baseline uses the nearest-neighbor classifier on the raw data, and its error rate is 6.5%. As can be seen, on this dataset, (1) our methods still outperform the counterparts. (2) our methods all perform better than the baseline, but not all the other 8 methods. This demonstrates that the GAE may discover more reasonable manifold structure by iteratively exploring the data relation. (3) From the error rates of kernel PCA (8.5%) and PCA (6.2%), it can be seen that the kernel extensions may not always improve the original methods, and finding a suitable kernel function is often the key issue. However, due to the multilayer neural network architecture, the proposed deep GAE has the universal approximation property [6], which can capture more complicated data structure.

4. Discussion and Conclusion

It is known that the denoising autoencoder [18] is trained to reconstruct a data from one of its corrupted versions.

Table 3. Performance comparison on the MNIST dataset. ER is short for "error rate". The reduced dimensions are in the parentheses. Our models use 30 dimensions. pp is short for "polyplus" kernel.)

Method	ER	Our Model	ER
PCA	6.2% (55)	dGAE-PCA	5.3%
Kernel PCA	8.5% (pp)		
LDA	16.1% (9)	dGAE-LDA	4.4%
Kernel LDA	4.6% (pp)		
ISOMAP	–	dGAE-ISOMAP	6.4%
LLE	–	dGAE-LLE	5.7%
LPP	7.9%(55)	dGAE-LE	4.3%
Kernel LPP	4.9% (pp)		
MFA	9.5% (45)	dGAE-MFA	3.9%
Kernel MFA	6.8% (pp)		

In the generalized autoencoder, a data is reconstructed by those in a specific set. From the denoising autoencoder view point, the GAE uses a set of "corrupted versions" for the reconstruction, such as its neighbors or the instances of the same class, instead of the versions with Gaussian noise or *masking noise* [18]. In the future, we will compare the generalized autoencoder with the denoising autoencoder on more tasks, such as feature learning and classification, and also consider incorporating of the merits of both.

As we know, the traditional autoencoder is an unsupervised method, which do not utilize class label. Classification restricted Boltzmann machine (ClassRBM) [7] may provide a solution to explicitly modeling class labels by fusing label vectors into the visible layer. However, training a neural network with such a visible layer needs a large amount of labeled data. We argue that the generalized autoencoder is able to exploit label information in learning more flexibly via using/selecting different data into the reconstruction sets. For example, we can build a reconstruction set according to the labels or just use nearest-neighbors by ignoring the labels, or even combining both strategies.

Acknowledgments

This work is jointly supported by National Basic Research Program of China (2012CB316300), Hundred Talents Program of CAS, and National Natural Science Foundation of China (61202328).

References

[1] M. Belkin and P. Niyogi. Laplacian eigenmaps and spectral techniques for embedding and clustering. *Advances in Neural Information Processing Systems*, 2002. 2, 3, 4, 5

[2] R. Duda, P. Hart, and D. Stork. Pattern classification, 2nd edition. *Wiley-Interscience, Hoboken, NJ*, 2000. 1, 3, 4, 6, 7

[3] X. He, D. Cai, S. Yan, and H. Zhang. Neighborhood preserving embedding. *International Conference on Computer Vision*, 2005. 2

[4] X. He and P. Niyogi. Locality preserving projections. *Advances in Neural Information Processing Systems*, 2004. 2, 5, 6, 7

[5] G. Hinton and R. Salakhutdinov. Reducing the dimensionality of data with neural networks. *Science*, 2006. 3, 4, 5, 6, 7

[6] K. Hornik. Multilayer feedforward networks are universal approximators. *IEEE Transactions on Neural Networks, vol. 2, pp. 359-366*, 1989. 7

[7] H. Larochelle, M. Mandel, R. Pascanu, and Y. Bengio. Learning algorithms for the classification restricted boltzmann machine. *Journal of Machine Learning Research, Vol. 13*, 2012. 8

[8] H. Lee, C. Ekanadham, and A. Ng. Sparse deep belief net model for visual area v2. *Advances in Neural Information Processing Systems*, 2008. 2

[9] K. Lee, J. Ho, M. Yang, and D. Kriegman. Video-based face recognition using probablistic appearance manifolds. *IEEE Conference on Computer Vision and Pattern Recognition*, 2003. 1

[10] K. Pearson. On lines and planes of closest fit to systems of points in space. *Philosophical Magazine*, 1901. 1, 3, 4, 6

[11] S. Rifai, P. Vincent, X. Muller, X. Glorot, and Y. Bengio. Contractive auto-encoders: Explicit invariance during feature extraction. *International Conference on Machine Learning*, 2011. 2, 3

[12] S. Roweis and L. Saul. Nonlinear dimensionality reduction by locally linear embedding. *Science*, 2000. 2, 3, 4, 5

[13] D. Rumelhart, G. Hinton, and R. Williams. Learning internal representations by error propagation. *Parallel Distributed Processing. Vol 1: Foundations. MIT Press, Cambridge, MA*, 1986. 2

[14] T. Sim, S. Baker, and M. Bsat. The cmu pose, illumination, and expression (pie) database. *Proc. IEEE Int'l Conf. Automatic Face and Gesture Recognition*, 2002. 5

[15] J. Tenenbaum, V. de Silva, and J. Langford. A global geometric framework for nonlinear dimensionality reduction. *Science*, 2000. 2, 3, 4, 5

[16] J. Venna, J. Peltonen, K. Nybo, H. Aidos, and S. Kaski. Information retrieval perspective to nonlinear dimensionality reduction for data visualization. *Journal of Machine Learning Research, Vol. 11*, 2010. 1

[17] R. Vidal, Y. Ma, and S. Sastry. Generalized principal component analysis (gpca). *IEEE Transactions on Pattern Analysis and Machine Intelligence, vol. 27, no. 12, pp. 1945-1959*, 2005. 1

[18] P. Vincent, H. Larochelle, Y. Bengio, and P. Manzagol. Extracting and composing robust features with denoising autoencoders. *International Conference on Machine Learning*, 2008. 2, 7, 8

[19] S. Yan, D. Xu, B. Zhang, H. Zhang, Q. Yang, and S. Li. Graph embedding and extensions: A general framework for dimensionality reduction. *IEEE Trans. on Pattern Analysis and Machine Intelligence*, 2007. 1, 2, 3, 4, 6, 7